# Formation Analysis for a Fleet of Drones: A Mathematical Framework

Emiliano Traversi[1], Michal Barcis[2], Lorenzo Bellone[2], Agata Barcis[2], Dina Ahmim-Bonaldi[2], Eliseo Ferrante[3] and Enrico Natalizio[2]

[1]*IDO Department, ESSEC Business School, Cergy-Pontoise, France*

[2]*Technology Innovation Institute, Abu Dhabi, U.A.E.*

[3]*New York University Abu Dhabi, Abu Dhabi, U.A.E.*

Keywords: Robot and Multi-Robot Systems, Task Planning and Execution, Formation Study.

Abstract: We consider a dynamic coverage scenario, where a group of agents (e.g., Unmanned Aerial Vehicles (UAVs)) is exploring an environment in search of a moving target (e.g., survivors on a lifeboat). We assume UAVs are capable to achieve, maintain, and move in formation (e.g., to maintain connectivity). This paper addresses the question "Which formation maximizes the chance of finding the target?". We propose a mathematical framework to answer this question. The proposed framework is generic and can be easily applied to various formations and missions. We show how the framework can identify which formation will result in better performance in the type of missions we consider. We analyze how different factors, namely the target speed relative to the group, affect the performance of the formations. We validate the framework against simulations of the considered scenarios. The supplementary video material including the real-world implementation is available at https://youtu.be/_mYmTnAJi-I?si=dSmVVNZOjj5NbSG1.

## 1 INTRODUCTION

Groups of agents or robots can be advantageous over single agents in several applications. Search missions (looking for survivors or faults or oil spills, etc.) constitute important applications and are also the subject of active research (Ivić et al., 2020). Deploying groups of searching agents can increase the efficacy and efficiency in such missions. An important decision is how to divide the search among agents. A possible choice is to divide the area into partitions and assign agents to independently explore them (Liu et al., 2023; Mazdin et al., 2020; Kovacina et al., 2002). In other situations, it may be advantageous to deploy search parties consisting of multiple agents to explore a common large area. For example, searching in groups can be advantageous when diverse capabilities are available within each search party (Dorigo et al., 2013). For autonomous (unmanned) searching agents, the need to travel in search parties is motivated by limited access to long-range communication devices: For instance, only some robots may be equipped with satellite modems allowing communication with the mission control station, while all robots are equipped with shorter range transceivers.

Agents employed in group search must travel in close proximity, but the exact relative positions of the agents vary. The specific choice of the set of relative positions of the agents can be referred to as a *formation*. Agents operating in formations present advantages: For instance, birds fly in specific formations to save energy (Bajec and Heppner, 2009), which inspired the development of systems that can reduce fuel consumption in aircrafts (Afonso et al., 2023; Antczak et al., 2022; Hartjes et al., 2019). Formation flights can also be used in the decentralized handling of control tasks for surveillance to optimize a system with respect to cost and weight constraints (Anderson et al., 2008). Formation control – the study on how to achieve and maintain a formation – is an active field of research (Justh and Krishnaprasad, 2002; Wang et al., 2007; Paul et al., 2008; Chao et al., 2012). The focus of our work is not on formation control. We instead assume a reliable method for formation control is already available.

The main hypothesis in this work is that some formations are better than others in group search missions, depending on the mission profile. We propose a mathematical model that can analyze how different choices of formation influence the target detection chance. We consider the dynamic coverage (Papatheodorou and Tzes, 2018; Atınç et al., 2020), or sweeping coverage (Cheng and Savkin, 2009; Zhai and Hong, 2012; Zhai and Hong, 2013; Saska et al., 2013) problem. To the best of our knowledge, we focus on the first time the effect of specific formation



Traversi, E., Barcis, M., Bellone, L., Barcis, A., Ahmim-Bonaldi, D., Ferrante, E. and Natalizio, E.
Formation Analysis for a Fleet of Drones: A Mathematical Framework.
DOI: 10.5220/0013189400003890

In *Proceedings of the 17th International Conference on Agents and Artificial Intelligence (ICAART 2025) - Volume 1*, pages 471-480
ISBN: 978-989-758-737-5; ISSN: 2184-433X

for intercepting a moving target.

The pursuer-evader task is related to the one considered in this paper (Hespanha et al., 1999). In (Yu et al., 2019; de Souza et al., 2021), multiple pursuers have been used to maximize their chances. In (Wei and Yanq, 2018), pursuers are used to lure the evader into their paths, while others simultaneously establish an encirclement to capture the target. In the above work, the pursuers' remain close to the evader, rather than finding it in an unknown environment.

In contrast to the above literature, this paper presents a different approach to dynamic coverage, focusing on the analysis of the use of different formations to search for a moving target with an unknown trajectory. The main contribution of this work is a mathematical framework for this analysis (Section 3). We validate the correctness of the framework in a simulated mission with Unmanned Aerial Vehicles (UAVs), and show a proof of concept with real UAVs (Section 4) where the framework can be useful. We conclude the paper in (Section 5).

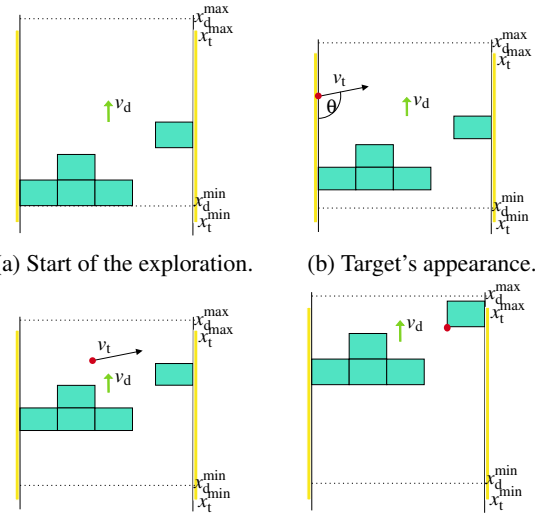


(a) Start of the exploration. (b) Target's appearance.

(c) Target follows trajectory. (d) Target is intercepted.

Figure 1: Example of a successful exploration.

## 2 PROBLEM STATEMENT

We consider a search mission in which a group of robots in formation has to find a moving target. We introduce a mathematical framework that models the effect of the formation on the search task. To simplify the mathematical treatment, we consider arbitrary linear search trajectories followed by the group of agents. We assume these are planned in a way to cover the parts of the environment where the target may appear. Each sweeping trajectory is modeled as a straight corridor depicted vertically: the agents traverse it from bottom to top. Let $n_d$ be the number of agents. Each agent is modeled as a rectangular area with size $\ell_h \times \ell_v$ that represents the agent field of view. If agents correspond to UAVs, the rectangular area represents the field of view of the camera equipped on the drone. The agents move within the corridor without changing their relative positions and at a constant speed of $v_d$. We assume a reference system that is fixed and centered on the group (in other words, the group does not move with respect to the considered reference frame). Figure 1 shows an illustrative example.

We introduce: The maximum and minimum entry points of the target, $x_t^{min}$ and $x_t^{max}$; The starting and ending points of agent exploration, $x_d^{min}$ and $x_d^{max}$.

The agent group has to detect the presence of a moving target within the corridor. The mission begins with the agents group positioned at the point $x_d^{min}$ (lower dotted horizontal lines in Figure 1), and it traverses the corridor at a constant speed $v_d$ up to the point $x_d^{max}$ (upper dotted horizontal lines in Figure 1). We assume that at any moment during the exploration, a target (represented as a red dot in Figure 1) enters the corridor from one of its edges at a randomly generated point within the interval $[x_t^{min}, x_t^{max}]$ (see the yellow left border in Figure 1) and with a random orientation (distributed in the range $[0, \pi]$), constant speed $v_t$, and following a straight trajectory. We indicate with $P_T(x)$ the probability that the target shows up at a given position $x \in [x_t^{min}, x_t^{max}]$.

During the exploration, if the target enters any of the agent's rectangular area, it is considered *intercepted*. If instead the target exits the other side of the corridor without entering any rectangle, it is considered *missed*. Furthermore, exploration stops when all agents have crossed the maximum exploration point, $x_d^{max}$. If the target has not been intercepted by that time, it is considered missed.

## 3 MODEL DEFINITION

In this section, we present the framework enables to compute the probability for a given group formation to intercept a target (hereby referred to as the *interception probability*) in a mission with a customizable profile.

### 3.1 Framework Overview

Let $x$ represent the distance between the target's entry point and the group of agents[1]. Define $S$ as the set of all subsegments of $[0,\pi]$, and $\mathcal{S}$ as the set of all subsets of $S$ (i.e., $\mathcal{S}$ is the power set of $S$). Key to our analysis is representing the set of *interceptable directions* $\mathcal{S}_x \subseteq \mathcal{S}$, that is the set of maximal (with respect to inclusion) segments that correspond to values of $\theta$ that lead to interception.

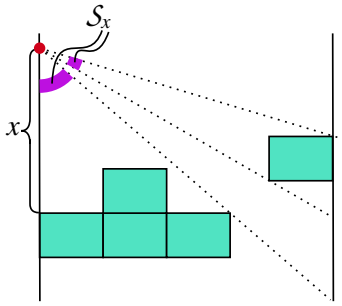


Figure 2: Example of $\mathcal{S}_x$ for a specific formation.

Figure 2 provides an example of $\mathcal{S}_x$ for a specific formation and distance $x$ between the formation and the target entry point (in red). Here, $\mathcal{S}_x$ contains the two segments in purple.

Let $P_x(\theta)$ be the probability that, for an entry point $x$, the direction of the target is equal to $\theta$ and let $P_x$ be the probability that the target is intercepted if it enters at a distance $x$ from the formation of agents. We can compute $P_x$ as:

$$P_x = \sum_{[\theta_1,\theta_2]\in\mathcal{S}_x} \int_{\theta_1}^{\theta_2} P_x(\theta)\, d\theta \tag{1}$$

In this equation, only entrance angles that belong to $\mathcal{S}_x$ and that yield to interceptions are integrated. Consider the case where all entry angles are equally probable ($P_x(\theta) = \frac{1}{\pi}$, $\forall\theta \in [0,\pi]$). In this case, $P_x$ (denoted as $\overline{P}_x$) is:

$$\overline{P}_x = \sum_{[\theta_1,\theta_2]\in\mathcal{S}_x} \int_{\theta_1}^{\theta_2} \frac{1}{\pi}\cdot d\theta = \frac{1}{\pi} \sum_{[\theta_1,\theta_2]\in\mathcal{S}_x} (\theta_2 - \theta_1)\ . \tag{2}$$

In the rest of the paper we will focus only on this case.

### 3.2 Modeling Formations

The type of formation selected impacts significantly the complexity of the description of the set $\mathcal{S}_x$. In this work, we focus on formations that allow the set $\mathcal{S}_x$ to have the following properties:

- *Symmetry*. $\mathcal{S}_x$ is symmetric if its value does not depend on the entry side of the target but only on the distance $x$. This property allows us to assume, without loss of generality, that the target enters from only one of the two sides.
- *Scalar-representability*. $\mathcal{S}_x$ is scalar-representable if it consists of one single segment of the form $[0,\theta_x]$. Loosely speaking, this holds when formations do not have "holes" in the range of angles $\theta$ that lead to interception. This property allows us to see $\mathcal{S}_x$ as a function $\mathcal{S}_x : \mathbb{R} \to [0,\pi]$ that for each entry point $x$ returns the maximal entry angle $\theta_x$ that leads to an interception. The entry point $x$ is to be understood as an absolute value, so the above holds regardless of whether the target enters in front or behind the formation.

Working with a set of interceptable directions that is symmetric and scalar-representable allows us to have a more tractable mathematical model. Having said this, the framework is general enough to be extendable also to the cases where "holes" are present.

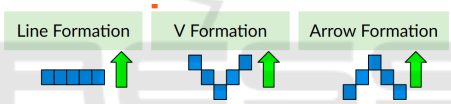


Figure 3: Formations considered.

Among the formations that meet the above properties, we study the three of them: *line*, *arrow*, and *vee* formations (see Fig. 3). We conclude by noting that the choice of the formation is not the only factor that can affect whether the set $\mathcal{S}_x$ is scalar representable or not, as it will become clear in the next section. Thus, conditions on the formation are necessary but not sufficient for having a scalar-representable set of interceptable directions.

### 3.3 Calculating $\overline{P}_x$

Except when explicitly stated, in the rest of this document we assume a set of interceptable directions $\mathcal{S}_x$ that is symmetric and scalar-representable. To make the analysis easier to tackle, we represent $\mathcal{S}_x$ as a composition of two functions, $f_D(\theta)$ and $f_S(x)$:

$$\mathcal{S}_x = [0, f_D(f_S(x))] \tag{3}$$

The function $f_S(x) : \mathbb{R} \to [0,\pi]$ (where the "S" stands for *static*) calculates the maximal entry angle at which we have an intersection between the target and the group of agents in a given formation, for a given snapshot of the mission whereby the agents do not

[1] In this paper we will denote by $x$ a position on the vertical axis. Depending on the context, it may indicate the target entry point or the position of the formation.

move (i.e., $v_d = 0$). This function takes into account the contribution of the specific formation but does not consider the magnitude of the speed of the target $v_t$ since agents are considered static ($v_d = 0$). The function $f_D(x) : [0,\pi] \to [0,\pi]$ (where the "D" stands for *dynamic*) models how the speed of the target $v_t$ and the speed of the agents $v_d$ modify the maximal entry angle calculated with $f_S(x)$.

Eq. (3) allows to simplify the computation of $\overline{P}_x$ (see Eq. (2)):

$$\overline{P}_x = \frac{1}{\pi} \sum_{[\theta_1,\theta_2] \in \mathcal{S}_x} (\theta_2 - \theta_1) = \frac{f_D(f_S(x))}{\pi} . \quad (4)$$

Eq. (4) shows that, if all target entry angles are equally probable, it is sufficient to determine the maximum entry angle for the given entry point and divide it by $\pi$ to obtain the probability of interception.

In the following, we detail how to calculate $f_D(\theta)$ and $f_S(x)$ for specific scenarios, as a guideline for applying the framework to any scenario with symmetric and scalar-representable $\mathcal{S}_x$.

### 3.3.1 Calculation of $f_S(x)$

We formalize the value of $f_S(x)$ as a function of the entry point of the target. According to the formation used, the definition will differ and incorporate the parameters $\ell_h$, $\ell_v$, and the size of the group $n_d$. For simplicity, we assume that we only consider an odd number of agents $n_d$ and we introduce $k$ that identifies the "'depth" of the formation $k = (n_d - 1)/2$.

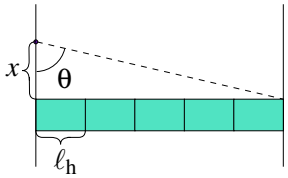


Figure 4: How to compute $f_S^L(x)$ for a line formation.

**Line-Formation.** The function $f_S(x)$ applied to a line formation is denoted as $f_S^L(x)$. Figure 4 shows how to calculate $f_S^L(x)$ by applying the definition of sine to the right triangle with vertices in the target entry point and in two extreme points of the formation:

$$f_S^L(x) = \arcsin\left(\frac{(2k+1)\ell_h}{\sqrt{(2k+1)^2\ell_h^2 + x^2}}\right) \quad (5)$$

If the reference system is defined appropriately, Eq. (5) can also be used for computing $f_S(x)$ when the target enters from the back of a line formation, in front of a vee-formation or from the back of an arrow-formation (see Fig. 5 for some examples).


(a) Target entering in the back of a line formation.

(b) Target entering in the front of a vee formation.

Figure 5: When to apply $f_S^L(x)$ to other configurations.

**Vee and Arrow Formations.** In this paragraph, we describe $f_S$ for a target entering in the front of an arrow formation and in the back of a vee formation, using the same equation thanks to symmetry. We denote it as $f_S^{AV}$ in both cases.

The more complex nature of the arrow and vee formations makes it necessary to split the analysis into three cases, depending on where the target hits the formation when it has a direction corresponding to its maximal entry angle: (1) The nearest side of the arrow (if $0 \le x \le k\ell_v$, see Figure 6a); (2) The "head" of the arrow (if $k\ell_v \le x \le (2k+1)\ell_v$, see Figure 6b); (3) The farthest side of the arrow (if $x \ge (2k+1)\ell_v$, see Figure 6c):

$$f_S^{AV}(x) = \begin{cases} \frac{\pi}{2} + \arcsin\left(\frac{k\ell_v - x}{\sqrt{(k\ell_v - x)^2 + k^2\ell_h^2}}\right) & 0 \le x \le k\ell_v \\ \arcsin\left(\frac{(k+1)\ell_h}{\sqrt{(k+1)^2\ell_h^2 + (x - k\ell_v)^2}}\right) & k\ell_v \le x \le (2k+1)\ell_v \\ \arcsin\left(\frac{(2k+1)\ell_h}{\sqrt{(2k+1)^2\ell_h^2 + x^2}}\right) & (2k+1)\ell_v \le x \end{cases} \quad (6)$$

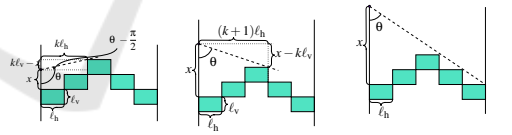


(a) Target touching the nearest side of the arrow.

(b) Target touching the head of the arrow.

(c) Target touching the farthest side of the arrow.

Figure 6: $f_S^{AV}(x)$ for different target entry points.

### 3.3.2 Calculation of $f_D(x)$

$f_D$ does not depend on the formation because it models how the maximum entry angle obtained in the static case is altered when the agents have a velocity greater than zero. Instead, $f_D$ depends on the entry point of the target. In the following, we indicate with $f_D^F(\theta)$ and $f_D^B(\theta)$ the values of $f_D$ when the target enters from the front or from the back.

If the agents are in motion, it becomes necessary to employ a formula that indicates how the speed of the target is perceived by the moving agents (recall

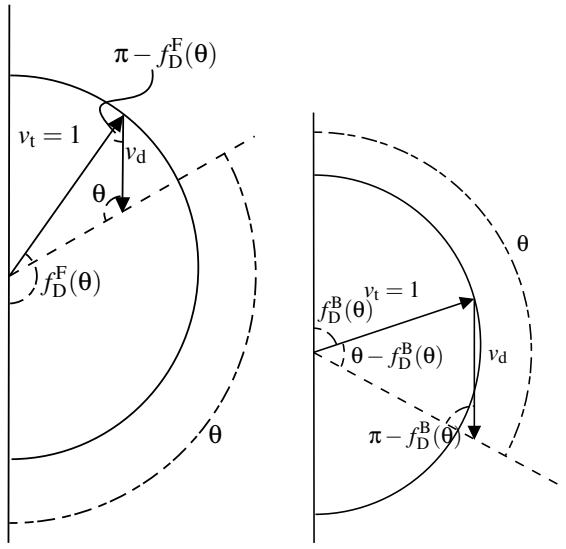


(a) Computation of $f_D^F(\theta)$ if the target enters in front of the agents.

(b) Computation of $f_D^B(\theta)$ if the target enters behind the agents

Figure 7: Computation of $f_D^F(\theta)$ and $f_D^B(\theta)$.

the reference system is fixed with the agent group). We observe that, when the target enters in front of the agents, moving agents increase the chances of intercepting the target, which corresponds to an increased maximum entry angle in the dynamic case. Similarly, when the target enters from the rear of the formation, the maximum entry angle also increases in the dynamic case.

The formulas for $f_D(\theta)$ do not depend on the exact values of the two velocities $v_t$ and $v_d$ but only on their ratio. For this reason, we suppose to have $v_t = 1$ w.l.o.g.

**Target Entering in Front of the Agents.** Figure 7a shows the quantities used to compute $f_D^F(\theta)$. We remind that the input of the function is the maximal entry angle in the static case (defined as $\theta$ in the figure) and that $v_d$ and $v_t$ are given as input. We can therefore use the law of sines to obtain the following relation:

$$\frac{v_d}{\sin\left(f_D^F(\theta) - \theta\right)} = \frac{1}{\sin(\theta)} \tag{7}$$

and therefore $f_D^F(\theta) = \theta + \arcsin(v_d \sin(\theta))$. The function arcsin is defined only in the interval $[-1,1]$, therefore we have the following constraint on the values of $\theta$: $-1 \leq v_d \sin(\theta) \leq 1$. If $v_d \leq 1$ then the inequalities are always satisfied. On the other hand, if $v_d > 1$ we have that $\theta \leq \arcsin\left(\frac{1}{v_d}\right)$, that has also a practical explanation: if the value of $v_d$ is high enough, regardless of the direction of the target and of the value of $\theta$, it will *always* be intercepted. We obtain:

$$f_D^F(\theta) = \begin{cases} \theta + \arcsin(v_d \sin(\theta)) & \text{if } v_d \leq 1 \\ & \text{or } \theta \leq \arcsin\left(\frac{1}{v_d}\right) \\ \pi & \text{otherwise} \end{cases} \tag{8}$$

that takes into account the values of $v_d$.

**Target Entering Behind the Agents.** In Fig. 7b we show how to compute $f_D^B(\theta)$. The law of sines leads to the following relation:

$$\frac{v_d}{\sin(\theta - f_D^B(\theta))} = \frac{1}{\sin(\pi - \theta)} \tag{9}$$

and therefore $f_D^B(\theta) = \theta - \arcsin(v_d \sin(\pi - \theta))$. The function arcsin is defined only in the interval $[-1,1]$, therefore we have that the only valid values for $\theta$ are the ones satisfying the following constraints: $-1 \leq v_d \sin(\pi - \theta) \leq 1$. If $v_d \leq 1$ then the inequalities are always satisfied. On the other hand, if $v_d > 1$ we have that $\theta \geq \pi - \arcsin\left(\frac{1}{v_d}\right)$. Similarly to the previous case, this requirement implies that if the value of $v_d$ is too high, regardless of the direction of the target and on the value of $\theta$, it will *never* be intercepted. We obtain:

$$f_D^B(\theta) = \begin{cases} \theta - \arcsin(v_d \sin(\pi - \theta)) & \text{if } v_d \leq 1 \\ & \text{or } \theta \geq \pi - \arcsin\left(\frac{1}{v_d}\right) \\ 0 & \text{otherwise} \end{cases} \tag{10}$$

that takes into account the values of $v_d$.

## 3.4 Modeling Missions

Once the formation and speeds of the agent fleet have been determined, the next step is to include the specific context of the mission within the model. This involves specifying the following parameters: the maximum and minimum entry points of the target ($x_t^{\min}$ and $x_t^{\max}$), the starting and ending points of agent exploration ($x_d^{\min}$ and $x_d^{\max}$), the probability ($P_x(\theta)$) that the angle associated with the direction of the target is equal to $\theta$, the speed of the target ($v_t$) and the probability $P_T(x)$ that the target enters the corridor when the fleet is at a given point $x$.

The choice of mission can significantly impact the complexity of calculating the corresponding interception probability. Therefore, in this paper we consider missions that are meaningful from an application standpoint and are also easily manageable from a formal perspective. Specifically, this involves searching for missions that possess the following property:

- *Scalar Representability*. Mission choice can change the way the set $\mathcal{S}_x$ is calculated. A mission is considered scalar-representable if it leads to a set of interceptable directions that is scalar-representable.

This is an example of another type of condition that is necessary to have a scalar-representable set $\mathcal{S}_x$, on top of those associated with the formation and presented in Section 3.2. In this work we consider scalar-representable missions, that is cases where $x_{\mathrm{d}}^{\max} = +\infty$, in other words where the fleet of agents can explore infinitely the corridor until either the target is intercepted or reaches the other side of the corridor. This assumptions allows to consider a target as missed only if its trajectory does not intercept an agent, regardless of where such an agent is intercepted.

To utilize the framework for comparing the advantages of one formation over another in a specific mission, an additional mathematical step is required. Specifically, we must calculate the integral of the target interception probabilities between the maximum and minimum entry points of the target (and possibly also between the starting and ending points of agent exploration). This calculation will subsequently yield the final interception probability for the given formation within the given mission context.

In Section 4, we will elaborate on these steps for validation purposes.

# 4 APPLICATION OF THE FRAMEWORK

In this section we first introduce $I^{\mathrm{F}}$ (resp. $I^{\mathrm{B}}$), the quantity that represents the integral of the punctual probability of intercepting the target entering in front (resp. in the back) of the drones up to a maximum distance that will be used in the mission considered. Intuitively, this value takes into account the fact that, while the drones are exploring, the distance where the target might appear in front (back) changes. By integrating various distances, $I^{\mathrm{F}}$ allows us to argue about the general performance of the mission.

Let $I^{\mathrm{F,L}}(x_{\mathrm{t}}^{\max})$ represent the integral of the probability of intercepting the target entering up to a maximum distance of $x_{\mathrm{t}}^{\max}$, in front of the drones flying in the line formation:

$$I^{\mathrm{F,L}}(x_{\mathrm{t}}^{\max}) = \frac{1}{\pi}\int_0^{x_{\mathrm{t}}^{\max}} f_{\mathrm{D}}^{\mathrm{F}}\left(f_{\mathrm{S}}^{\mathrm{L}}(x)\right) dx\,. \tag{11}$$

Similarly, we can define the quantities $I^{\mathrm{B,L}}(x_{\mathrm{t}}^{\max})$, $I^{\mathrm{F,AV}}(x_{\mathrm{t}}^{\max})$ and $I^{\mathrm{B,AV}}(x_{\mathrm{t}}^{\max})$ where F stands for *front* and B stands for *back* of the formation, while L stands for *line* formation and AV stands for either *arrow* or *vee* formation.

## 4.1 Mission Description

We select two scalar-representable missions, called *entry-time aware* and *entry-time agnostic*. They differ on the assumptions on the probability $P_{\mathrm{T}}(x)$ that the target enters the corridor when the fleet is at a given point $x$.

**Entry-Time Aware Missions.** The basic idea of this mission is that the fleet is alerted to the entry of a target and consequently already begins to move. This assumption translates in practice to the assumption that the target enters the corridor at instant $t = 0$ at a uniformly distributed random distance within the range $[0, x_{\mathrm{C}}]$, where $x_{\mathrm{C}}$ is the length of the corridor.

The main variable is the position of the fleet when the target arrives. We therefore define as $P^{\mathrm{awe}}(x)$ the probability of intercepting the target in an entry-time aware environment when the fleet is at position $x \in [0, x_{\mathrm{C}}]$. When the formation is at a distance $x$ from the beginning of the corridor, the probability of intercepting the target for a line formation $P_{\mathrm{L}}^{\mathrm{awe}}(x)$ is equal to:

$$P_{\mathrm{L}}^{\mathrm{awe}}(x) = \frac{1}{x_{\mathrm{C}}}\left(I^{\mathrm{F,L}}(x_{\mathrm{C}} - \ell_{\mathrm{v}} - x) + 1\cdot\ell_{\mathrm{v}} + I^{\mathrm{B,L}}(x)\right)\,. \tag{12}$$

The computation of $P_{\mathrm{L}}^{\mathrm{awe}}(x)$ consists of three components, the first computes the contribution associated to the case where the target enters in front of the formation, the middle one takes into account the fact that the target can enter "touching" the formation and the third component takes into account the contribution due to the target entering in the back of the formation.

Similarly, for the arrow and vee formations we have:

$$P_{\mathrm{A}}^{\mathrm{awe}}(x) = \frac{1}{x_{\mathrm{C}}}\left(I^{\mathrm{F,AV}}(x_{\mathrm{C}} - \ell_{\mathrm{v}} - x) + 1\cdot\ell_{\mathrm{v}} + I^{\mathrm{B,L}}(x)\right) \tag{13}$$

$$P_{\mathrm{V}}^{\mathrm{awe}}(x) = \frac{1}{x_{\mathrm{C}}}\left(I^{\mathrm{F,L}}(x_{\mathrm{C}} - \ell_{\mathrm{v}} - x) + 1\cdot\ell_{\mathrm{v}} + I^{\mathrm{B,AV}}(x)\right)\,. \tag{14}$$

**Entry-Time Agnostic Missions.** For these missions we assume that we do not know the exact time of entrance of the target, we only assume that it will enter while the fleet of drones is moving. We assume that the drones start flying at $t = 0$ at the bottom of the corridor and fly through the corridor up to its end. The target can enter at any time during the movement. Let

$P_{\mathrm{L}}^{\mathrm{agn}}$ be the probability of interception for an entry-time agnostic mission of a line formation. The formula for computing $P_{\mathrm{L}}^{\mathrm{agn}}$ reduces to the integral over the whole corridor of the quantity $P_{\mathrm{L}}^{\mathrm{awe}}$, where $P_{\mathrm{T}}(x)$ is the probability that the target enters at distance $x$. For this mission, we assume that $P_{\mathrm{T}}(x)$ is uniform and therefore it can be considered constant, leading to the following calculation:

$$P_{\mathrm{L}}^{\mathrm{agn}} = \int_0^{x_{\mathrm{C}}-\ell_{\mathrm{v}}} P_{\mathrm{L}}^{\mathrm{awe}}(x)\,dx = \frac{1}{x_{\mathrm{C}}^2}\int_0^{x_{\mathrm{C}}-\ell_{\mathrm{v}}} (I^{\mathrm{F,L}}(x_{\mathrm{C}}-\ell_{\mathrm{v}}-x)+1\cdot\ell_{\mathrm{v}}+I^{\mathrm{B,L}}(x))\,dx$$

and for the other two formations we have:

$$P_{\mathrm{A}}^{\mathrm{agn}} = \int_0^{x_{\mathrm{C}}-\ell_{\mathrm{v}}} P_{\mathrm{A}}^{\mathrm{awe}}(x)\,dx = \frac{1}{x_{\mathrm{C}}^2}\int_0^{x_{\mathrm{C}}-\ell_{\mathrm{v}}} (I^{\mathrm{F,AV}}(x_{\mathrm{C}}-\ell_{\mathrm{v}}-x)+1\cdot\ell_{\mathrm{v}}+I^{\mathrm{B,L}}(x))\,dx$$

$$P_{\mathrm{V}}^{\mathrm{agn}} = \int_0^{x_{\mathrm{C}}-\ell_{\mathrm{v}}} P_{\mathrm{V}}^{\mathrm{awe}}(x)\,dx = \frac{1}{x_{\mathrm{C}}^2}\int_0^{x_{\mathrm{C}}-\ell_{\mathrm{v}}} (I^{\mathrm{F,L}}(x_{\mathrm{C}}-\ell_{\mathrm{v}}-x)+1\cdot\ell_{\mathrm{v}}+I^{\mathrm{B,AV}}(x))\,dx\,.$$

## 4.2 Simulation-Based Validation

To assess the validity of the mathematical framework presented in Section 3, we implemented a lightweight simulator using Python. It allows us to define multiple moving entities and control them through velocity and yaw rate input. We used it to simulate a fleet of aerial agents and the moving target that are present in the two missions presented in Section 4.1. Each aerial agent is equipped with a detection sensor, which provides the capability of detecting a target if it falls within a certain rectangular area simulating the sensor's field of view. This area corresponds to the visual range of a real-world camera-equipped drone.

With the agents in formation, the fleet starts to move in a direction within a fixed space interval. During the mission, the target can appear at different moments, according to the analyzed mission. A target will be considered detected if it falls within the visual range of at least one aerial agent during the mission.

In order to carry out a fair comparison between simulation and mathematical framework, we ran several missions in different conditions. In detail, each experiment is parametrized with the following variables: i) fleet velocity, ii) target's starting point, iii) target's heading, and iv) target's appearance time. While the model considers these parameters as continuous variables, in simulation we uniformly sample each of them in 150 instances for the entry-time aware, and 24 instances for the entry-time agnostic mission. The introduction of an additional variable in the entry-time agnostic scenario significantly increases the computation time. Hence, the choice to reduce the sampling rate for this case allowed us to fix the simulation time to a given maximum (i.e., around 4 hours).

The validation of the mathematical framework is carried out by analyzing the same scenario both in simulation and using the framework. For each of them, we compute the probability of successful target detection at different ratios between target and fleet velocity. Eventually, we expect to get similar results using both simulation and the mathematical framework. The parameters of the missions considered are reported in Table 1. The simulations were run on a workstation with an Intel(R) Core(TM) i9-10980XE processor running at 3.00 GHz.

Table 1: Parameters of the considered scenarios used in both mathematical framework and simulation.

| Parameter | Value |
|---|---|
| Corridor length | 1 km |
| Detection range | 90 m × 67.5 m |
| Formation width | 450 m |
| Arrow/Vee formation height | 202.5 m |
| Maximum fleet velocity | 10 m/s |
| Target velocity | 5 m/s |

The results from the validation are presented in Fig. 8. Each subfigure displays the probability of successful target detection as a function of the ratio between target and fleet velocities. Qualitatively, the same trend in performance for both mathematical framework and simulation stands out. The discrepancy between the plot obtained with the mathematical framework and the simulation performance never exceeds 1.2 ppt for the entry-time aware and 2.3 ppt for the entry-time agnostic missions, which is expected due to a slight discrepancy between the theoretical assumptions and the simulator. Such similar results between our framework and the simulation demonstrate that the mathematical model is able to properly assess the performance of different formations in both of the presented scenarios. At the same time, it allows for almost immediate computation of results, in contrast to the simulation used for validation, which takes significant time to complete.

## 4.3 Extended Results with the Framework

We used the framework to obtain additional insights into the proposed scenarios. To do so, we use the

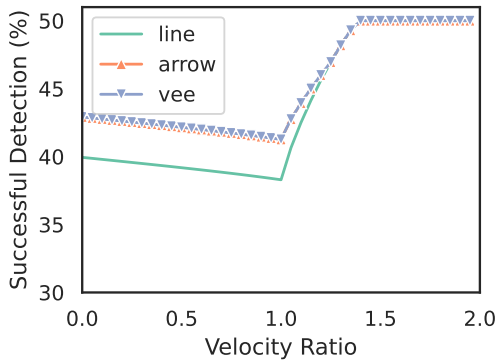


(a) Mathematical framework results, entry-time aware mission

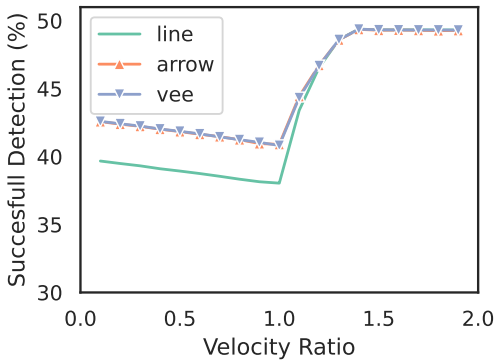


(b) Simulation results, entry-time aware mission

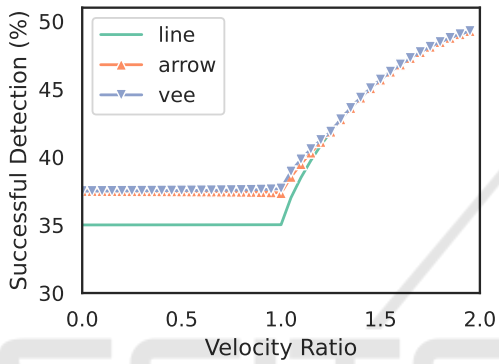


(c) Mathematical framework results, entry-time agnostic mission

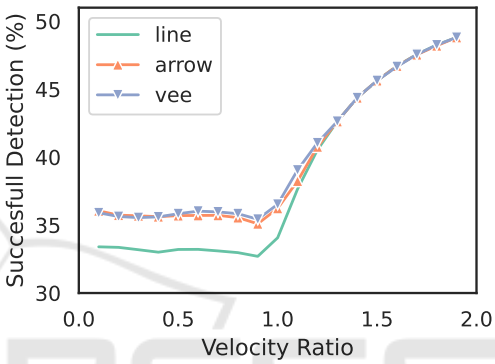


(d) Simulation results, entry-time agnostic mission

Figure 8: Comparisons of mathematical framework vs simulation results for entry-time aware and agnostic missions.

mathematical framework to calculate the aforementioned probabilities in various scenarios.

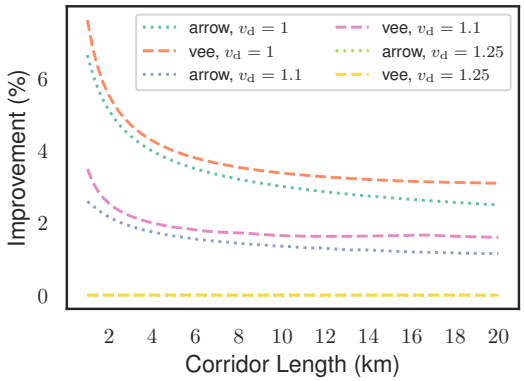


Figure 9: Results of the experiment showing how the performance depends on the length of the corridor. The vertical axis shows the relative improvement of detection chance wrt to the line formation.

To support the reproducibility of our research, we publish the source code of the mathematical framework and of this study in [redacted in initial submission to maintain anonymity]. We start by analyzing the results presented in Fig. 8. First of all, for both scenarios, the vee formation results in the best performance, being slightly better than the arrow formation. The line formation performing significantly worse. Furthermore, in both cases, the formations achieve the same performance starting from a velocity ratio of around 1.25, which confirms the intuition that for fast-moving search parties, the formation choice is less important. For the velocity ratio above 1.5, they converge to the 50% of successful detections. This observation matches the intuition that, with high speed, the 50% of the targets that appear in front of the formation will all be detected before they can escape from the fleet detection range. Furthermore, the results of the entry-time aware mission present a perhaps counter-intuitive finding: if the searching drones cannot move as fast as the target, it might be better to slow them down even further. This can be explained by the fact that moving slower gives more chances for the targets appearing behind the formation to catch up with the formation and the formation will not be able to catch up to many targets appearing in front of

it. This behavior does not appear in the entry-time agnostic mission, where a target entrance time is included.

In Fig. 9 we show how the performance in the entry-time agnostic mission changes depending on the corridor length. We present it as a relative improvement wrt to the line formation to emphasize the benefits of choosing the correct formation. We show the plots for multiple values of $v_d$ to show how this plot changes in relation to the findings previously presented in Fig. 8. The obtained results are very intuitive: the longer the corridor, the lower the benefit of choosing the better formation.

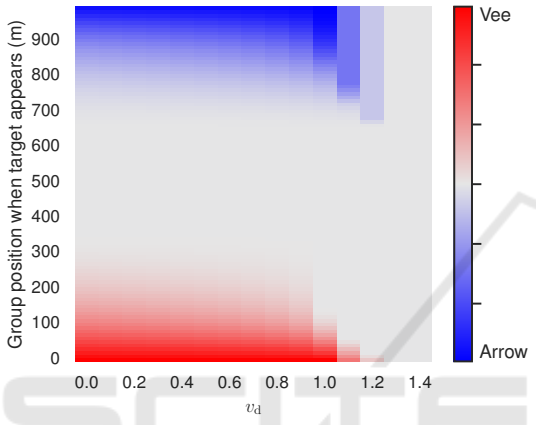


Figure 10: Results of the experiment showing which formation outperforms the other according to different velocity ratios and positions of the group when the target appears.

Finally, to explicitly address the question presented as the motivation of this research, we present Fig. 10. It presents the difference in performance between the vee and arrow formation and could serve as an easy way to choose which one to prefer, depending on the scenario at hand. The line formation is not presented, as it is never performing better than the aforementioned two.

### 4.4 Robotic Proof of Concept

Our proof of concept involves deploying a fleet of six UAVs (specifically, Holybro PX4 Vision) in each of the formations introduced above. The UAVs are equipped with Arducam 12 MP, IMX477 camera with an 80° horizontal field of view, flying at an altitude of 50 meters with an exploration depth (corridor length) of 1 kilometer. This setup was successfully tested over a maritime environment to detect a target in the sea and in a deserted area to detect a car using a YOLO algorithm (Redmon et al., 2016), demonstrating that our model is applicable in realistic scenarios.

## 5 CONCLUSIONS

The mathematical framework presented in this paper offers a convenient and efficient means of analyzing the formation flights of a fleet of drones. It allows for the estimation of the probability of target detection during a search mission. Specifically, it serves as a valuable tool for selecting the most effective formation in a given context. The proposed scenarios demonstrate the practical value of this framework in real-world applications such as search and rescue, border surveillance, and environmental monitoring. Although our initial experiments yielded promising results, we are planning further in-field experiments to gain insights and quantitatively validate the mathematical framework under realistic conditions and across various scenarios.

## REFERENCES

Afonso, F., Sohst, M., Diogo, C. M. A., Rodrigues, S. S., Ferreira, A., Ribeiro, I., Marques, R., Rego, F. F. C., Sohouli, A., Portugal-Pereira, J., Policarpo, H., Soares, B., Ferreira, B., Fernandes, E. C., Lau, F., and Suleman, A. (2023). Strategies towards a more sustainable aviation: A systematic review. *Progress in Aerospace Sciences*, 137:100878.

Anderson, B. D., Fidan, B., Yu, C., and Van der Walle, D. (2008). UAV Formation Control: Theory and Application. In *Recent advances in learning and control*, volume 371 of *Lecture Notes in Control and Information Sciences*, pages 15–33. Springer edition.

Antczak, A., Lasek, M., and Sibilski, K. (2022). Efficient Positioning of Two Long-Range Passenger Aircraft in Formation Flight. *Transactions on Aerospace Research*, Nr 3 (268).

Atınç, G. M., Stipanović, D. M., and Voulgaris, P. G. (2020). A swarm-based approach to dynamic coverage control of multi-agent systems. *Automatica*, 112:108637.

Bajec, I. L. and Heppner, F. H. (2009). Organized flight in birds. *Animal Behaviour*, 78(4):777–789.

Chao, Z., Zhou, S.-L., Ming, L., and Zhang, W.-G. (2012). UAV Formation Flight Based on Nonlinear Model Predictive Control. *Mathematical Problems in Engineering*, 2012:e261367. Publisher: Hindawi.

Cheng, T. M. and Savkin, A. V. (2009). Decentralized coordinated control of a vehicle network for deployment in sweep coverage. In *2009 IEEE International Conference on Control and Automation*, pages 275–279. ISSN: 1948-3457.

de Souza, C., Newbury, R., Cosgun, A., Castillo, P., Vidolov, B., and Kulić, D. (2021). Decentralized Multi-Agent Pursuit Using Deep Reinforcement Learning. *IEEE Robotics and Automation Letters*, 6(3):4552–4559. Conference Name: IEEE Robotics and Automation Letters.

Dorigo, M., Floreano, D., Gambardella, L. M., Mondada, F., Nolfi, S., Baaboura, T., Birattari, M., Bonani, M., Brambilla, M., Brutschy, A., Burnier, D., Campo, A., Christensen, A. L., Decugniere, A., Di Caro, G., Ducatelle, F., Ferrante, E., Forster, A., Gonzales, J. M., Guzzi, J., Longchamp, V., Magnenat, S., Mathews, N., Montes de Oca, M., O'Grady, R., Pinciroli, C., Pini, G., Retornaz, P., Roberts, J., Sperati, V., Stirling, T., Stranieri, A., Stutzle, T., Trianni, V., Tuci, E., Turgut, A. E., and Vaussard, F. (2013). Swarmanoid: A Novel Concept for the Study of Heterogeneous Robotic Swarms. *IEEE Robotics & Automation Magazine*, 20(4):60–71. Conference Name: IEEE Robotics & Automation Magazine.

Hartjes, S., Visser, H. G., and van Hellenberg Hubar, M. E. G. (2019). Trajectory Optimization of Extended Formation Flights for Commercial Aviation. *Aerospace*, 6(9):100. Number: 9 Publisher: Multidisciplinary Digital Publishing Institute.

Hespanha, J., Kim, H. J., and Sastry, S. (1999). Multiple-agent probabilistic pursuit-evasion games. In *Proceedings of the 38th IEEE Conference on Decision and Control (Cat. No.99CH36304)*, volume 3, pages 2432–2437 vol.3. ISSN: 0191-2216.

Ivić, S., Crnković, B., Arbabi, H., Loire, S., Clary, P., and Mezić, I. (2020). Search strategy in a complex and dynamic environment: the MH370 case. *Scientific Reports*, 10:19640.

Justh, E. W. and Krishnaprasad, P. S. (2002). A Simple Control Law for UAV Formation Flying.

Kovacina, M., Palmer, D., Yang, G., and Vaidyanathan, R. (2002). Multi-agent control algorithms for chemical cloud detection and mapping using unmanned air vehicles. In *IEEE/RSJ International Conference on Intelligent Robots and Systems*, volume 3, pages 2782–2788 vol.3.

Liu, H. Y., Chen, J., Huang, K. H., Cheng, G. Q., and Wang, R. (2023). UAV swarm collaborative coverage control using GV division and planning algorithm. *The Aeronautical Journal*, 127(1309):446–465. Publisher: Cambridge University Press.

Mazdin, P., Barciś, M., Hellwagner, H., and Rinner, B. (2020). Distributed Task Assignment in Multi-Robot Systems based on Information Utility. In *2020 IEEE 16th International Conference on Automation Science and Engineering (CASE)*, pages 734–740. ISSN: 2161-8089.

Papatheodorou, S. and Tzes, A. (2018). Theoretical and Experimental Collaborative Area Coverage Schemes Using Mobile Agents.

Paul, T., Krogstad, T. R., and Gravdahl, J. T. (2008). Modelling of UAV formation flight using 3D potential field. *Simulation Modelling Practice and Theory*, 16(9):1453–1462.

Redmon, J., Divvala, S., Girshick, R., and Farhadi, A. (2016). You Only Look Once: Unified, Real-Time Object Detection. arXiv:1506.02640 [cs].

Saska, M., Vonásek, V., and Přeučil, L. (2013). Trajectory Planning and Control for Airport Snow Sweeping by Autonomous Formations of Ploughs. *Journal of Intelligent & Robotic Systems*, 72(2):239–261.

Wang, X., Yadav, V., and Balakrishnan, S. N. (2007). Cooperative UAV Formation Flying With Obstacle/Collision Avoidance. *IEEE Transactions on Control Systems Technology*, 15(4):672–679. Conference Name: IEEE Transactions on Control Systems Technology.

Wei, X. and Yanq, J. (2018). Optimal Strategies for Multiple Unmanned Aerial Vehicles in a Pursuit/Evasion Differential Game. *Journal Guidance, Control and Dynamics*, 41.

Yu, Y., Li, Z., Wang, X., and Shen, L. (2019). Bearing-only circumnavigation control of the multi-agent system around a moving target. *IET Control Theory & Applications*, 13(17):2747–2757.

Zhai, C. and Hong, Y. (2012). Decentralized sweep coverage algorithm for uncertain region of multi-agent systems. In *2012 American Control Conference (ACC)*, pages 4522–4527. ISSN: 2378-5861.

Zhai, C. and Hong, Y. (2013). Decentralized sweep coverage algorithm for multi-agent systems with workload uncertainties. *Automatica*, 49(7):2154–2159.